Journal of
Synchrotron
Radiation

ISSN 0909-0495

Received 22 October 2012
Accepted 9 January 2013

# A feasibility study of dynamic stress analysis inside a running internal combustion engine using synchrotron X-ray beams

**Nikolaos Baimpas,[a]* Michael Drakopoulos,[b] Thomas Connolley,[b] Xu Song,[a] Costas Pandazaras[c] and Alexander M. Korsunsky[a]**

[a]Department of Engineering Science, University of Oxford, Parks Road, Oxford OX1 3PJ, UK, [b]Diamond Light Source, Harwell Science and Innovation Campus, Didcot, Oxfordshire OX11 0DE, UK, and [c]Department of Mechanical Engineering, University of Thessaly, Volos, Leoforos, Athinon, Pedion Areos 383 34, Greece. E-mail: nikolaos.baimpas@eng.ox.ac.uk

The present investigation establishes the feasibility of using synchrotron-generated X-ray beams for time-resolved *in situ* imaging and diffraction of the interior components of an internal combustion engine during its operation. The demonstration experiment was carried out on beamline I12 (JEEP) at Diamond Light Source, UK. The external hutch of the JEEP instrument is a large-scale engineering test bed for complex *in situ* processing and simulation experiments. The hutch incorporates a large capacity translation and rotation table and a selection of detectors for monochromatic and white-beam diffraction and imaging. These capabilities were used to record X-ray movies of a motorcycle internal combustion engine running at 1850 r.p.m. and to measure strain inside the connecting rod *via* stroboscopic X-ray diffraction measurement. The high penetrating ability and high flux of the X-ray beam at JEEP allowed the observation of inlet and outlet valve motion, as well as that of the piston, connecting rod and the timing chain within the engine. Finally, the dynamic internal strain within the moving connecting rod was evaluated with an accuracy of $\sim 50 \times 10^{-6}$.



**Keywords: internal combustion engine; live X-ray imaging; time-resolved diffraction; experimental stress analysis.**

## 1. Introduction and background

The knowledge of multi-component spatially and temporally varying stress–strain states and structural information is crucial for developing and validating models of engineering components and assemblies. The internal combustion engine is a multi-part complex thermomechanical machine consisting of numerous components and delivering the combination of power density and overall power that has ensured its un-diminishing popularity for over a century of exploitation. The ignition of the fuel–air mixture inside the combustion chamber causes a rise in gas temperature and pressure, thus generating a force on the pistons that is transmitted through connecting rods (con-rods) to cause the rotation of the crankshaft and producing exploitable mechanical torque. Complete analysis of the engine operation for the purposes of performance evaluation and optimization takes into account gas cycle measurements within the cylinder and incorporates information about flow rates, gas pressure and temperature, and structure vibration and stress. Comprehensive thermo-mechanical models of the engine need to be validated against experimental measurements, before they can be fully accepted as useful predictive tools used for design and optimization.

A variety of sensors and data logging devices are used to obtain measurements of the engine operating parameters. For example, thermocouples can be embedded in the cylinder block to record the temperature history, and strain sensors can be used to obtain measures of deformation at the surface of the assembly. These methods are capable of providing both time-resolved and location-specific measures. However, obtaining similar temporally and spatially resolved information *non-destructively* from *inside* the operating combustion engine is a much greater challenge. The harsh mechanical and thermal environment presents a significant challenge for conventional sensor systems.

X-ray beams available at high-energy third-generation synchrotron sources possess a range of special properties, such as brightness, tunability and coherence. For the purpose of the engineering feasibility study presented here we were principally interested in the combination of penetration ability and

high flux. The former property ensures that it is possible to 'see' through relatively large metallic assemblies, such as an internal combustion engine. More specifically, X-ray beams that have been transmitted through or diffracted from internal components must possess sufficient intensity for efficient detection, providing a fast and spatially resolved measure of the internal arrangement of components and their deformation.

In the present investigation we were interested in imaging the movement of the con-rod attached to the reciprocating piston, together with the valves regulating air inlet and exhaust. We also wished to investigate the feasibility of mapping the spatial distribution of internal elastic strains in the moving con-rod. Evidently, this kind of spatially resolved measurement also has to be sufficiently fast, since the stress distribution varies continuously over the period of crankshaft revolution.

It is important to emphasize that the principal benefit of the proposed methodology is that it can serve model validation and design optimization for internal combustion engines, ultimately helping improve fuel efficiency, power output, reliability, and also reduction of the amount and weight of material used.

In service, a single con-rod experiences repeated loading that runs to a high number of cycles ($10^8$–$10^9$). The type of loading ranges from compression induced by the pressure of combustion gases on the piston to tensile and bending loads due to inertial phenomena. Finite-element-analysis simulations (Shenoy & Fatemi, 2006) have been formulated in order to predict the dynamic multi-axial stress response of con-rods in service. However, the fidelity of such models depends strongly on the availability of correct boundary conditions and other data, such as the time-dependent temperature and pressure of combustion products. A number of further unknown parameters remain, namely those related to friction, the engine's response to external load (*e.g.* the forces that arise from road interaction) and the complex coupling between the engine's mechanical performance and ancillary systems (cooling, oil and fuel circuits). These aspects of the problem introduce further challenges for finite-element simulation and necessitate additional characterization *via* dynamic experimental measurements in operating internal combustion engines. Strain gauges can be attached to the con-rod and used to acquire continuous deformation data to be captured and transmitted or stored (Shenoy, 2004; Manner, undated; CompactRIO, undated). However, this approach suffers from the limitations associated with strain gauges being sensitive to temperature and thermal gradients, as well as the engine vibrations and the difficulty of connecting signal wires to data loggers at high revolutions per minute (r.p.m.) (Ishida *et al.*, 1995).

The non-destructive nature of X-ray imaging and diffraction is a highly effective means of visualizing internal structures at different spatial resolutions (Buffiere *et al.*, 1999), and for mapping internal residual and 'live' strain distributions (Korsunsky *et al.*, 2002). Alongside the classical powder diffraction mode, various approaches have been proposed for probing inter- and intra-granular deformation within crystalline materials (Poulsen *et al.*, 2001; Tamura *et al.*, 2003). The variety of techniques and arrangements that have been put forward (Sharma *et al.*, 2012; Daymond *et al.*, 2007; Efstathiou *et al.*, 2010; Thomas *et al.*, 2006; San Martin *et al.*, 2012) allows the selection of length scales (from a few millimetres down to submicrometres) and obtaining information about various material properties (local or statistical crystal orientation, crystallographic phase composition). In particular, high-energy polychromatic beam configuration for elastic strain measurement allows fast data acquisition and lends itself well to the mapping of large sample areas (Korsunsky *et al.*, 2002). At Diamond Light Source (DLS) I12, a Canberra 23-element germanium energy-dispersive X-ray detector (EDXD) is used for polychromatic powder diffraction measurements.

X-ray imaging, microscopy, topography and tomography techniques have witnessed rapid development in recent years, due to the advent of improved beam-conditioning optics and detectors offering better efficiency and resolution. X-ray imaging has a broad field of applications through being able to visualize the internal structure within complex-shaped objects. Radiography as well as tomography techniques make use of the penetrating ability of X-ray beams that show differential attenuation depending on the integral mass absorption coefficient along the beam path. Whilst micrometre resolution can now be achieved routinely using scintillators coupled to magnifying optics, achieving nanoscale ($\sim$100 nm) resolution requires special set-ups making use of curved (divergent) beam geometries (Stampanoni *et al.*, 2009). In addition, submillisecond time resolution can be achieved using rapid imaging (Rack *et al.*, 2009), for example through using imaging devices such as the Vision Research Phantom v7.3 CMOS high-speed camera (Vision Research, undated).

### 1.1. Experiment preparation and planning

At the initial preparatory stage of the experiment, composite ('mosaic') radiographic images of the engine block assembly were collected at different crankshaft rotation angles (0–120°) while the engine remained stationary. This allowed beam attenuation by the engine assembly to be evaluated, and the conditions for imaging to be established.

This was followed by 'live' imaging of the movement of the valves, as well as the motion of the con-rod–piston assembly. 'Live' strain state at a single point on the engine con-rod was then evaluated by a stroboscopic diffraction technique (Plech *et al.*, 2003), through synchronization of the fast electronic shutter of the EDXD detector with the engine crankshaft angular position, and accumulating the signal over multiple engine cycles.

The possibility of carrying out the experiment was contingent on resolving a number of previously unaddressed issues:

(i) X-ray beams undergo strong attenuation when passing through metallic assemblies. Successful data collection requires the engine to be sufficiently radiographically 'transparent' for the beam to penetrate simultaneously the engine block, the piston skirt and the con-rod, whilst allowing the

**Table 1**
Honda ATC engine specifications.

| | |
|---|---|
| Engine type | Four-stroke, air-cooled |
| Displacement | 124 cc |
| Bore × stroke | 55.0 × 52.2 mm |
| Compression ratio | 8.8–1 |
| Compression | 156–198 p.s.i. |
| Transmission speeds | Four-speed with dual range |
| Final drive | Chain |

exposure times to remain sufficiently short (<10 ms for a single-shot exposure). The engine side-view must not be obscured by other moving components, such as the flywheel, timing chain or the complex cooling water circuit channels. For the purposes of con-rod bending stress analysis, the incoming beam should be parallel to the pin end of the piston, so that the translation of the assembly across the beam would allow high spatial resolution across the con-rod for strain scanning. A typical single-cylinder air-cooled motorcycle engine does not have any of the above limitations, and has an overall lightweight construction. It was chosen as a system that satisfies all the above requirements. The cooling fins forming the engine-block outer shell are made from cast Al alloy with a low absorption coefficient. The steel piston skirt has a relatively small thickness (<3 mm), and the con-rod with the I-beam cross-section has a maximum width of 7 mm at the side brackets. The configuration of the Honda ATC engine finally chosen for investigation is shown in Table 1. The attenuation of the X-ray beam during its passage through the engine is illustrated on a cross section of the engine in Fig. 1(*a*) (Hubbell, 1982).

(ii) The engine was securely mounted on the test bed available in the external hutch (EH2) of the JEEP instrument (Fig. 1*b*), using a rigid support structure and minimizing the vibration effects that would cause blurring during image acquisition and uncertainty in the gauge volume position during diffraction measurements. The configuration was made ready for assembly within the restricted time-frame of the experiment. For these reasons a complete motorcycle configuration was selected, as it combined the rigidity of the frame with the fact that it already accommodates important ancillary components of the engine (exhaust, fuel tank, electrics *etc.*). A tricycle Honda ATC 125M was used, together with the specially designed self-standing frame that provided a convenient base for further bracing and mounting on the test bed of the hutch. Additional bracing of the motorcycle frame and shielding the engine moving parts ensured minimal vibration effects and safety in the hutch. The engine mounting arrangement on the test bed *via* a steel base frame is shown in Fig. 1(*b*), together with the wheel safety covers.

(iii) The time-resolved nature of the experiment required precise monitoring of the reciprocating piston movement and the ability to trigger data acquisition (in both imaging and diffraction modes) at specific crank angles, with a high degree of repeatability over consecutive strokes. Signal accumulation was used to achieve sufficient intensity. To synchronize detector triggering with the crankshaft angular position,

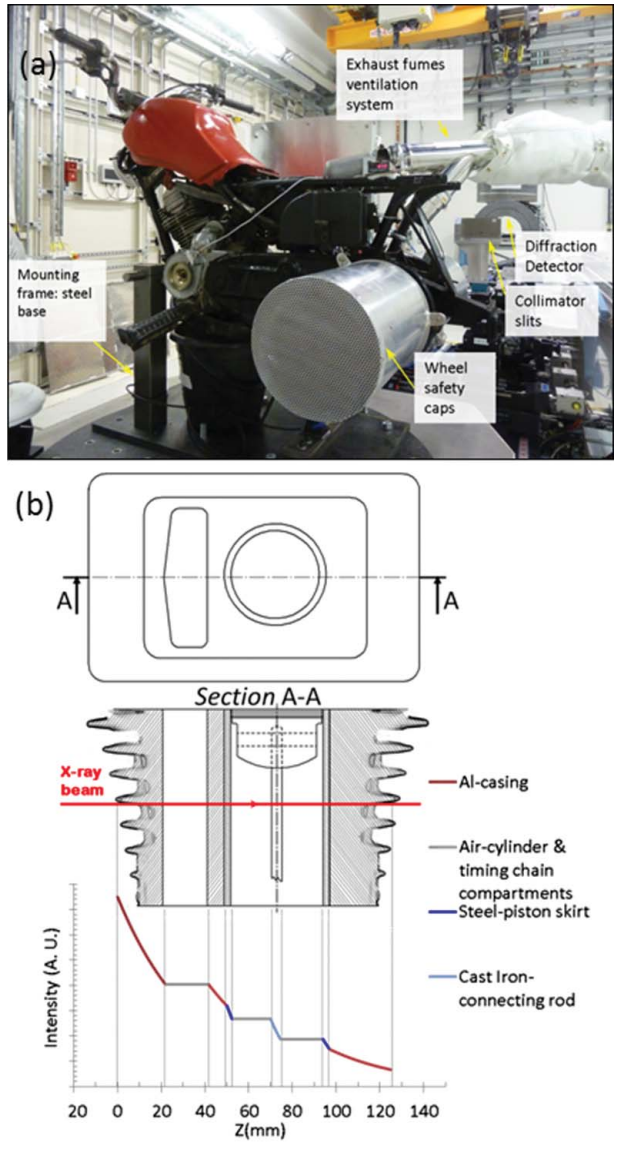


**Figure 1**
(*a*) Running motorcycle frame mounted on the high-capacity sample-positioning table of the rig inside EH2, I12, DLS. (*b*) Beam attenuation through the engine cross section. The position of the cross section *A*–*A* is demonstrated at the top of the figure. The cast Al attenuation is shown in red, the steel-piston skirt attenuation in blue, the cast iron con-rod in cyan and air attenuation in grey. The absorption coefficient $\mu$ for each metal is taken from NIST for energy 150 keV and the attenuation is according to the Beer–Lambert law.

electronic gating arrangements were put in place. A proximity sensor, connected to a tachometer, was mounted on the motorcycle crankshaft and emitted a TTL square signal pulse every time the piston reached the top dead centre (TDC). The tachometer was able to register the input frequency up to 7.5 kHz and delivered a pulse to a waveform generator that emitted a new TTL pulse with (*a*) specific delay time, (*b*) specific pulse width and (*c*) total cycle period. The delay time was determined from the frequency of rotation of the engine (r.p.m.) according to the desired shaft angle for observation on the con-rod. A specific location was chosen for detailed analysis, corresponding to the distance from the pin end of

20 mm. The width of the TTL timing pulse was determined by the desired exposure time of the detector. This was chosen to ensure that the displacement of the con-rod during exposure amounted to less than three pixels of the imaging camera (nominal pixel size 30.30 µm × 30.30 µm). This was adopted as a good compromise between achieving sufficient accumulated counts and accuracy of position and gauge volume definition. Due to the engine being a four-stroke engine, the detectors were triggered at half the frequency of the crankshaft rotation, to ensure consistent sampling of the engine cycle. A schematic diagram of the triggering configuration is shown in Fig. 2.

### 1.2. Set-up

The insertion device at beamline I12 at Diamond Light Source, Harwell Oxford Campus, Didcot, UK, is a liquid-He-cooled superconducting multiple wiggler with a peak magnetic field of 4.2 T, built by the Budker Institute of Nuclear Physics in Novosibirsk, Russia. Permanent filters are mounted in the beam to reduce heat load, to provide beam hardening and to act as vacuum windows: two 1.1 mm-thick CVD diamond windows are used for primary filtering, and a 4 mm CVD SiC window is used as a secondary filter. This provides a useful X-ray spectrum in the range 50–150 keV (Korsunsky *et al.*, 2010).

The motorcycle set-up as illustrated in Fig. 1(*b*) was installed in experimental hutch 2 of I12 JEEP. Exhaust fumes were pumped to the outside of the hutch through a ventilation system capable of removing ∼1500 l min$^{-1}$ of exhaust gas at temperatures up to 573 K. A flow regulator (damper valve circuit) was used to regulate the system intake when the engine was not producing the amount of exhaust fumes that the pump was extracting, thus allowing natural flow of the engine outtake stroke. On similar engine test rigs the fume extractor is usually not attached to the engine, as the engine typically operates in a dedicated isolated chamber. However, in this experiment the vent was fixed to the exhaust system to protect the equipment in the experimental hutch.

For imaging, a broad-spectrum white beam with a cross section of 18 mm × 24 mm was directed at the engine. The transmission image through the engine was registered using an X-ray camera consisting of a scintillator ($CdWO_4$) that was coupled to visible-light optics and a high-speed CMOS camera (Vision Research Phantom V7.3). The Module 1 imaging set-up used corresponded to a nominal pixel size (accounting for point spread function) of ∼30 µm and a field of view of 17.8 × 23.8 mm.

For diffraction, the 23-element energy-dispersive 'horse-shoe' detector was used. The individual detector elements on the detector are arranged at equal azimuthal steps on a half circle. The detector was aligned with respect to the incident beam to ensure the equal scattering angle of 10° for all elements. To improve the scattering angle definition, collimating slits were placed in front of each detector element. Details of the collimation system can be found elsewhere (Korsunsky *et al.*, 2010). The incoming beam together with the set of slits define a gauge volume of approximate dimensions

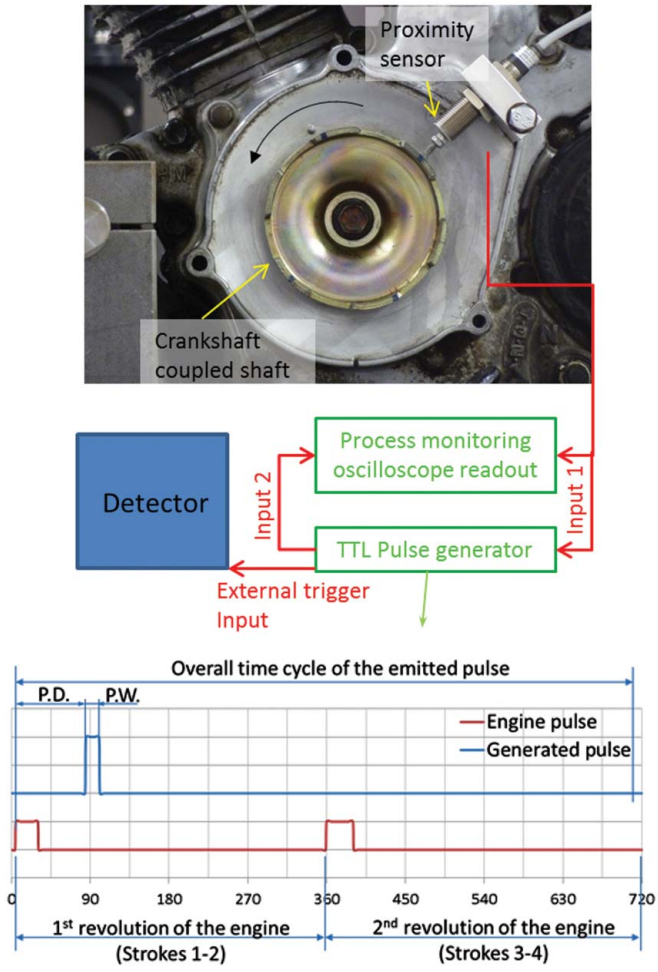


**Figure 2**
Schematic illustration of the detector triggering set-up. A pulse is triggered every 360°, by the proximity sensor mounted on the rotating shaft mounted on a 1:1 ratio to the crankshaft. The pulse is fed to the TTL pulse generator and the process monitoring oscilloscope. The parameters, such as pulse delay (P.D.) that controls the angular position we are hitting the con-rod according to the r.p.m., *i.e.* phase, and the pulse width (P.W.) which controls the exposure time, *i.e.* the time that the shutter of the detector remains open on every cycle, are adjusted. The overall time cycle of the emitted pulse is set just under the duration of two overall crankshaft revolutions to ensure triggering on the same stroke each time.

0.1 mm × 0.1 mm across the beam and ∼2.1 mm along the beam (Fig. 3*a*) (Rowles, 2011). At the set-up stage the position of the con-rod in the plane perpendicular to the incident beam was aligned using the imaging mode of the beamline. For the subsequent local strain measurements the beamline was configured for diffraction. The correct position of the gauge volume with respect to the con-rod was confirmed through prior X-ray imaging and through three-dimensional alignment scans in diffraction mode. The final alignment in diffraction mode was carried out by scanning through the entire cross section of the con-rod along the directions $AA'$, $BB'$, $CC'$ and $DD'$ (Fig. 3*b*). The scan results were used to confirm that the gauge volume position and the beamline positioning arrangements were in good agreement with the engineering model of the engine.

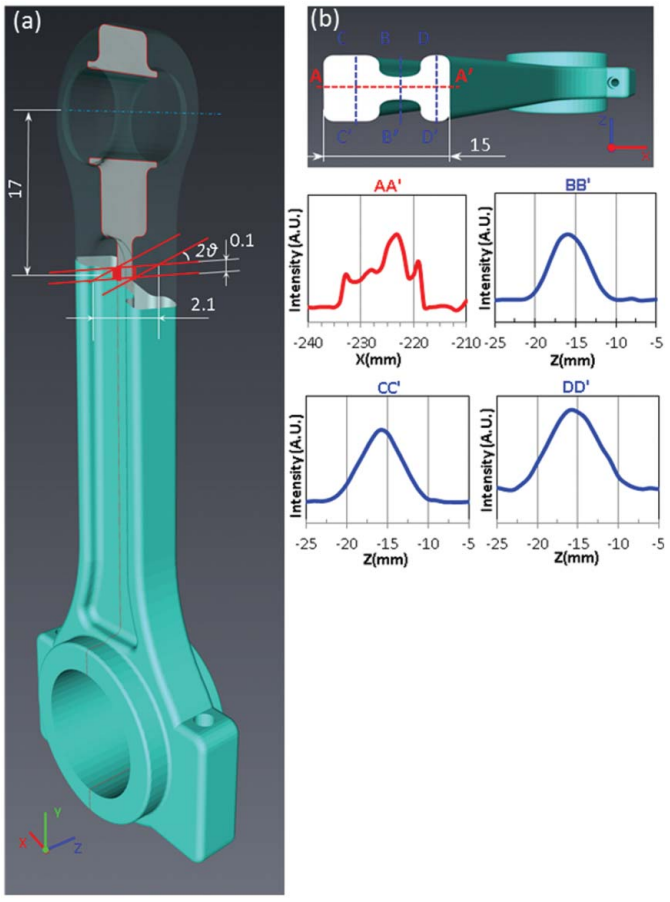


**Figure 3**
(*a*) Schematic of the con-rod diffraction set-up. The inclined cross section shows the angle at which the con-rod stands with respect to the *Y*-axis of the set-up in I12. Highlighted in red is the cross-sectional definition of the gauge volume defined by the double set of collimation slits and the incident beam cross-sectional size (0.1 × 2.1 mm). (*b*) Cross section of the plane analysed by diffraction 17 mm below the pin end of the con-rod. Highlighted in red is the *x*-scan used to determine the overall width of the section, and blue indicates the *z*-scan to locate the gauge volume in the middle of the con-rod. Scans in *x* (*AA*′) and *z* (*BB*′, *CC*′, *DD*′) show the integrated intensity from all channels of the EDXD detector. The observed intensity variation comes from the combination of absorption and scattering power (polycrystalline structure) of the material within the gauge volume.

## 2. Results

### 2.1. Live X-ray imaging of engine cylinder

'Live' imaging of the cylinder operation was initially carried out in 'one-shot' mode. Since the number of photons available for imaging in this case is severely restricted by the short exposure time, the signal-to-noise levels are high. In Fig. 4 the inherent background noise structure of the Phantom camera can be distinguished. The larger compound image in Fig. 4 shows reduced contrast and resolution. The outline of the piston pin is barely visible, suggesting that stroboscopic accumulation of images is likely to be required for the collection of high-resolution data.

Fig. 5 shows a sequence of cylinder valve images during engine operation. In the sequence taken at intervals of 20° phase angle, the valve enters the field of view from above,

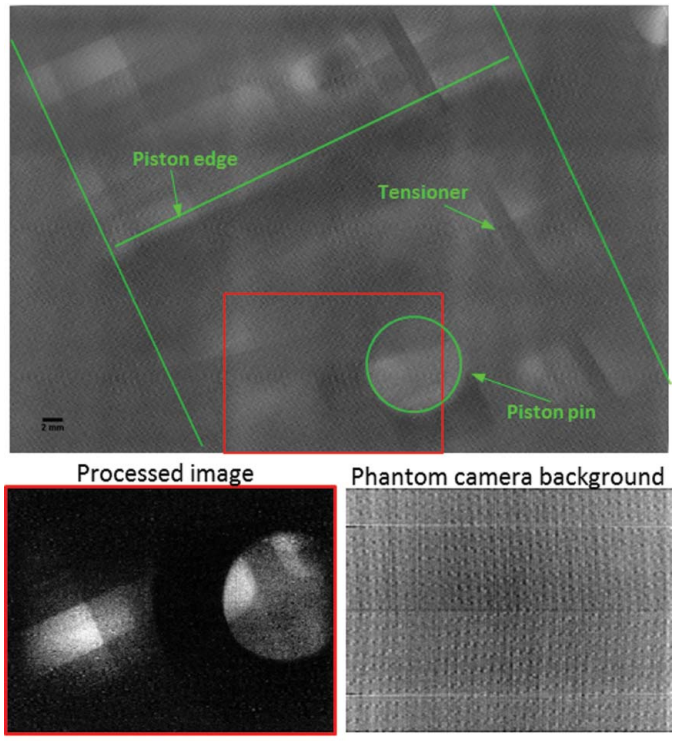


**Figure 4**
Mosaic of the engine's cross-section map at 120° crankshaft rotation at 1850 r.p.m. (delay time: 10.8 ms; exposure time: 500 µs).

reaches the lowest position near the middle of the image, and is withdrawn again upwards. Acceptable spatial resolution of the image was obtained, sufficient to distinguish the valve profile. The video version of this sequence is available as supplementary material.[1]

### 2.2. Compound radiography of engine in operation

Fast radiographic image collection was carried out in stroboscopic accumulation mode. To achieve this, the triggering procedure described above was used to control the Phantom high-speed camera, and the images were added to improve the signal-to-noise ratio. Owing to the limited field of view compared with the size of the object and region of interest, 'tiling' of images was required in order to build up an overall picture of the operating engine. For that purpose the high-capacity high-precision sample-positioning table in the external hutch of JEEP was used to drive the engine to different imaging positions whilst keeping the combustion running. Detector triggering ensured that images taken at different times corresponded to the same phase of engine rotation. Some variation in beam intensity and detector response with time was observed, *i.e.* different sub-images had different overall intensity. Some beam profile non-uniformity across the field of view was evident. In order to build up the overall radiographic picture of the engine at a particular phase

[1] Supplementary data for this paper are available from the IUCr electronic archives (Reference: CN5042). Services for accessing these data are described at the back of the journal.

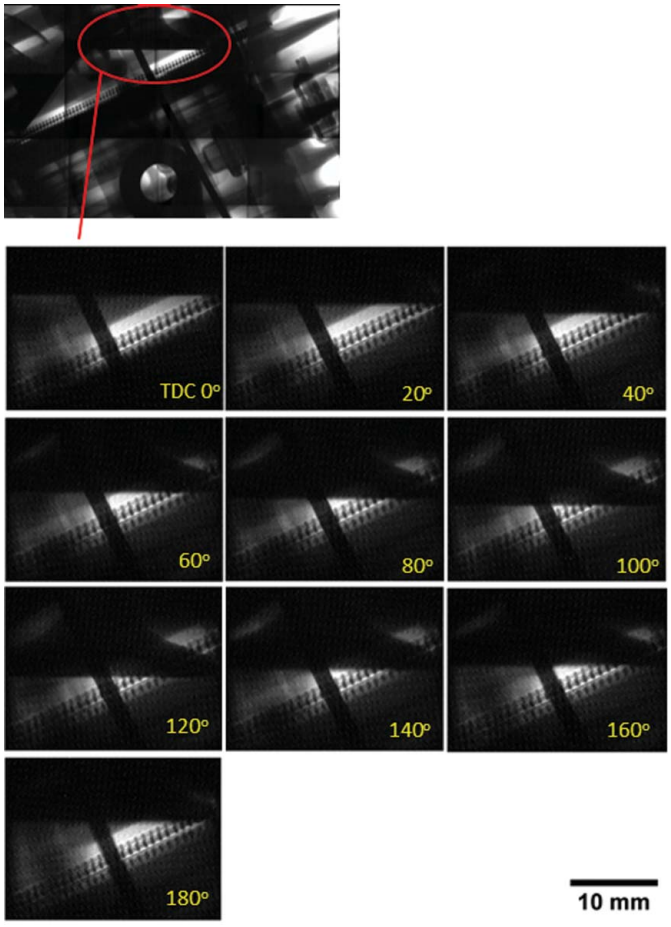


**Figure 5**
Image sequence from the intake valve starting at the TDC piston position at 20° crankshaft rotation increments, showing significant wear of the camshaft lobes at 1850 r.p.m. (exposure time: 1 ms). The shape of the lobes was found severely distorted due to ageing or poor lubrication, thus preventing the intake valve from dropping further into the cylinder from angles 60° to 140°.

instance during its operation, some image intensity correction was applied. This was accomplished by edge matching between individual adjacent tiles, seeking to ensure a consistent compound image. The overall composite ('mosaic') image is shown in Fig. 6. It displays excellent contrast, good sharpness (absence of blurring) and therefore good spatial resolution of engine internal features. The details of the timing chain, gears, internal threads and also the moving crankshaft are all clearly distinguishable.

### 2.3. Strain analysis

Diffraction of hard X-rays from polycrystalline materials is well established as a truly non-destructive spatially and directionally resolved measurement method for elastic lattice strain, allowing the macroscopic and microscopic components of stress to be deduced.

'Live' strain measurements carried out in the present study had a spatial resolution of <0.1 mm and a time resolution of <1 ms. The beam was collimated to the size 0.1 mm × 0.1 mm

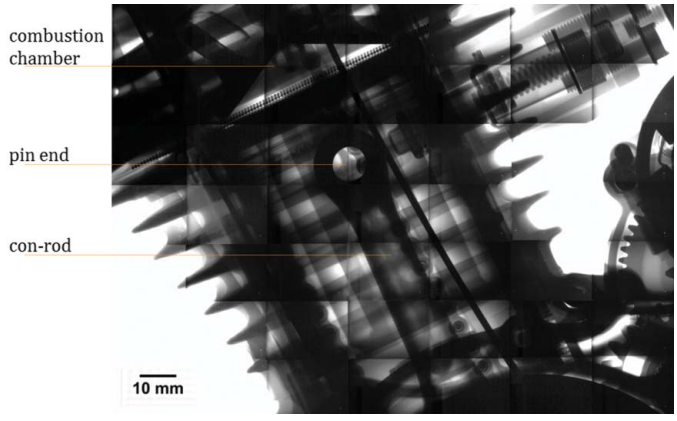


**Figure 6**
Mosaic of the engine cross-section assembly close to 0° crankshaft rotation (top dead centre, TDC).

located at the position on the crankshaft shown in Fig. 7, lying 17 mm below the piston pin axis. The measured strain direction is also illustrated on the schematic. Energy-dispersive diffraction data were collected in stroboscopic mode, by adding diffraction patterns corresponding to the same phase over multiple engine operating cycles. For the cast iron material of the con-rod (*Im*3*m* crystal structure, unstrained lattice parameter ∼2.852 Å), four peaks (200, 211, 220, 310) were analysed, as indicated in Table 2. A stationary reference residual stress linear profile across the con-rod was first collected. The *in situ* pattern showed no additional peak broadening compared with the data collected from a static

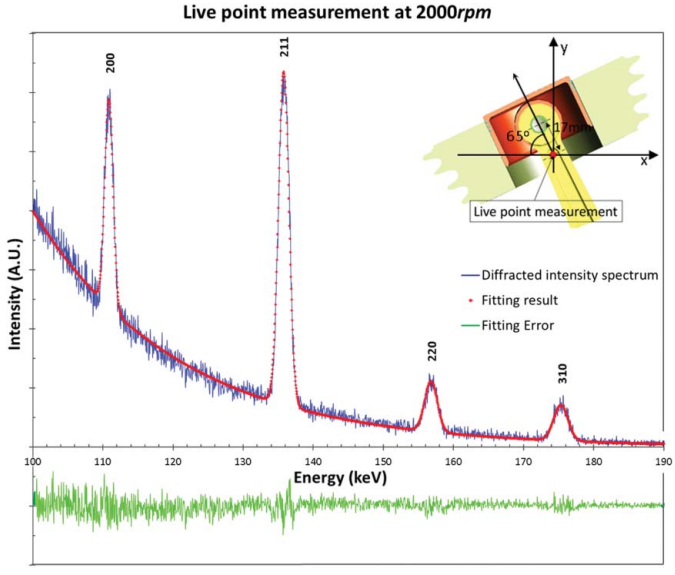


**Figure 7**
Illustration of the multi-peak fitting result together with the fitting error shown by the bottom curve. CAD schematic representation of the engine assembly cross section, with the point where the diffraction measurement was taken highlighted in red. It shows the 65° azimuthal positioning of the cylinder with respect to the laboratory coordinates. At 0° of crankshaft rotation (TDC) the perpendicular strain direction on the con-rod is parallel to the cylinder. For that reason the spectrum collected from channel No. 8 of the Ge detector (at 65.4° azimuthal angle) was used for the determination of strain along the reciprocating motion direction.

**Table 2**
*d*-spacing values (Å) and peak centre (keV) for the cast iron generated peaks.

| *h* | *k* | *l* | *d* (Å) | Peak centre (keV) |
|---|---|---|---|---|
| 2 | 0 | 0 | 1.4241 | 110.8852 |
| 2 | 1 | 1 | 1.1627 | 135.8061 |
| 2 | 2 | 0 | 1.0070 | 156.8154 |
| 3 | 1 | 0 | 0.9006 | 175.3249 |

engine. Fig. 7 illustrates the result of diffraction profile fitting using the Pawley refinement method. The background was fitted with a second-order polynomial. The green line below the plot in Fig. 7 indicates the fitting error, confirming that satisfactory agreement was achieved. The derived strain was found to be ~630 microstrains (compressive) at 0° during the ignition stroke at ~2000 r.p.m.

Fig. 8 shows detail of fitting for the 211 peak of ferrite located at 135.7203 keV (*d*-spacing = 1.1634 Å). The curve for the stationary con-rod pattern corresponds to the data points shown by red '+' markers. The 211 peak for the 'live' measurement had the centre located at 135.8061 keV (*d*-spacing = 1.1627 Å), and corresponds to the data points shown by blue '+' markers. The peak positioning error for the pattern taken from the stationary engine was only ~30 p.p.m. ($30 \times 10^{-6}$). A long exposure time of 3000 s was used for this measurement to achieve maximum precision. The peak shown in Fig. 8 was extracted from the diffraction pattern collected when the engine was running. The exposure time for each revolution was 0.289 ms with total accumulated exposure time amounting to ~24 s during 80 min overall engine running time. The accuracy of determining the peak centre position was better than 40 p.p.m. ($40 \times 10^{-6}$). The strain calculation from interplanar lattice spacings computed on the basis of peak centre positions in the reference and 'live' patterns ($d_0$ and $d$, respectively) is accomplished simply as

$$\varepsilon = \frac{d - d_0}{d_0}. \quad (1)$$

Based on the above formula, the strain in the con-rod during operation was found to be compressive and equal to 630 microstrain ($630 \times 10^{-6}$). The accuracy of experimental strain evaluation was thus consistently better than 50 microstrain ($50 \times 10^{-6}$), as illustrated in Fig. 8. This corresponds to the nominal stress evaluation result of ~120 ± 10 MPa. The small error of only ~10 MPa provides the proof of feasibility of 'live' stress–strain analysis in a running internal combustion engine.

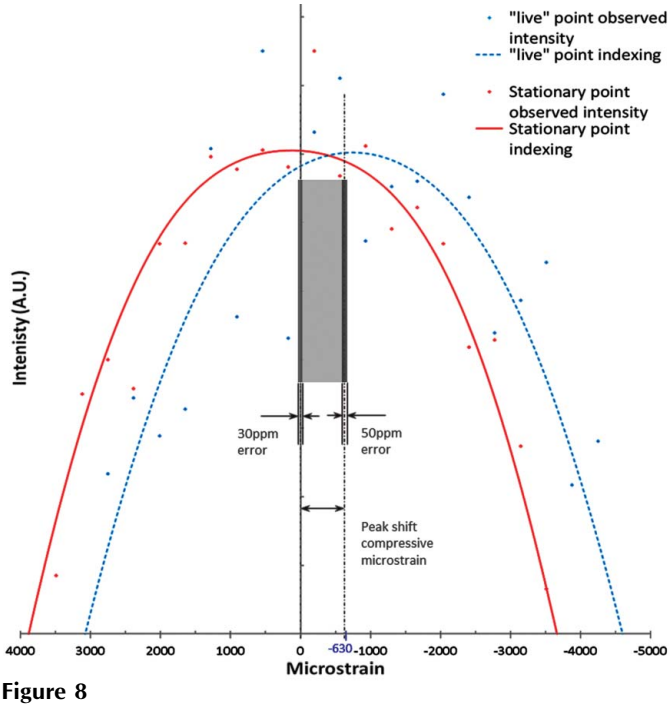


**Figure 8**
Close-up illustration of the 211 peak fitting result for 'live' measurement in blue and stationary measurement in red. The peak intensities are normalized so that they have the same intensity height distribution. The peak positioning error for the stationary measurement is 30 p.p.m. and for the 'live' measurement is 50 p.p.m. The measured compressive strain (630 microstrain) represented by the peak shift is highlighted in light grey colour and the peak positioning error margins are highlighted in dark grey colour. [See also the supplementary figure, which shows a mosaic of the engine cross section assembly at 120° crankshaft rotation (inverted greyscale colourmap).]

## 3. Conclusion and outlook

The results of the feasibility study presented in this report concern the combination of imaging and scattering from internal components of an operating internal combustion engine for non-destructive determination of component motion and strain.

The results open at least two avenues for further strain analysis. One makes use of the contrast achieved in the imaging mode, and in principle allows displacement mapping to be performed by digital image correlation (Sutton *et al.*, 1983). Differentiation of displacement maps with respect to time allows speeds to be measured, whilst differentiation with respect to position provides data on the distribution of total strain in engine components. However, since the elastic strains are typically small (<1%), this method is likely to be best suited to situations when plastic deformation is observed. The second approach that is particularly important for the determination of microscale and residual stresses is polycrystalline diffraction which relies on elastic strain evaluation through precise determination of interplanar lattice spacing by diffraction.

Further development of the ideas outlined in the present study is envisaged in terms of establishing close coupling between modelling of the engine operation (precise geometric representation of component shape; modelling the thermodynamics and fluid dynamics of gas flow through the engine; incorporation of inertia effects in deformation) and experimental model validation.

The work described above was carried out under the umbrella of the Centre for In Situ Processing Studies (CIPS) located at the Research Complex at Harwell (RCaH) and supported by the EPSRC under grant EP/I020691/1. The

authors are grateful to Diamond Light Source for beam time provision under allocation EE6958, and to the entire team at I12 JEEP for their support.

## References


Buffiere, J.-Y., Maire, E., Cloetens, P., Lormand, G. & Fougeres, R. (1999). *Acta Mater.* **47**, 1613–1625.

CompactRIO (undated). *Developing an Engine Connecting Rod Fatigue Test System Based on Compact RIO*, http://sine.ni.com/cs/app/doc/p/id/cs-14705.

Daymond, M. R., Young, M. L., Almer, J. D. & Dunand, D. C. (2007). *Acta Mater.* **55**, 3929–3942.

Efstathiou, C., Boyce, D. E., Park, J. S., Lienert, U., Dawson, P. R. & Miller, M. P. (2010). *Acta Mater.* **58**, 5806–5819.

Hubbell, J. (1982). *Int. J. Appl. Radiat. Isot.* **33**, 1269–1290.

Ishida, S., Hori, Y., Kinoshita, T. & Iwamoto, T. (1995). *SAE Tech. Pap.* 951797 (doi:10.4271/951797).

Korsunsky, A. M., Collins, S. P., Owen, R. A., Daymond, M. R., Achtioui, S. & James, K. E. (2002). *J. Synchrotron Rad.* **9**, 77–81.

Korsunsky, A. M., Song, X., Hofmann, F., Abbey, B., Xie, M. Y., Connolley, T., Reinhard, C., Atwood, R. C., Connor, L. & Drakopoulos, M. (2010). *Mater. Lett.* **64**, 1724–1727.

Manner, E. (undated). *Continuous Acquisition of Measuring Data up to an Enviromental Temperature of 180°C (Temperature, Deformation, Pressure between Piston Rings)*, http://www.sensortelemetrie.de/fileadmin/user_upload/Downloads/Vertriebsunterlagen/Motormesstechnik_en.pdf.

Plech, A., Kurbitz, S., Berg, K. J., Graener, H., Berg, G., Gresillon, S., Kaempfe, M., Feldmann, J., Wulff, M. & von Plessen, G. (2003). *Europhys. Lett.* **61**, 762–768.

Poulsen, H. F., Nielsen, S. F., Lauridsen, E. M., Schmidt, S., Suter, R. M., Lienert, U., Margulies, L., Lorentzen, T. & Juul Jensen, D. (2001). *J. Appl. Cryst.* **34**, 751–756.

Rack, A., García-Moreno, F., Baumbach, T. & Banhart, J. (2009). *J. Synchrotron Rad.* **16**, 432–434.

Rowles, M. R. (2011). *J. Synchrotron Rad.* **18**, 938–941.

San Martin, D., Jiménez-Melero, E., Duffy, J. A., Honkimäki, V., van der Zwaag, S. & van Dijk, N. H. (2012). *J. Appl. Cryst.* **45**, 748–757.

Sharma, H., Huizenga, R. M. & Offerman, S. E. (2012). *J. Appl. Cryst.* **45**, 693–704.

Shenoy, P. S. (2004). PhD thesis, University of Toledo, USA.

Shenoy, P. S. & Fatemi, A. (2006). *J. Mech. Eng. Sci.* **220**, 615–624.

Stampanoni, M., Marone, F., Mikuljan, G., Jefimovs, K., Trtik, P., Vila-Comamala, J., David, C. & Abela, R. (2009). *J. Phys. Conf. Ser.* **186**, 012018.

Sutton, M. A., Wolters, W. J., Peters, W. H., Ranson, W. F. & McNeil, S. R. (1983). *Image Vis. Comput.* **1**, 133–139.

Tamura, N., MacDowell, A. A., Spolenak, R., Valek, B. C., Bravman, J. C., Brown, W. L., Celestre, R. S., Padmore, H. A., Batterman, B. W. & Patel, J. R. (2003). *J. Synchrotron Rad.* **10**, 137–143.

Thomas, O., Loubens, A., Gergaud, P. & Labat, S. (2006). *Appl. Surf. Sci.* **253**, 182–187.

Vision Research (undated). *Phantom v7.3 High-Speed Camera*, http://www.visionresearch.com/Products/High-Speed-Cameras/v73/.